Transitions of tethered polymer chains: A simulation study with the bond fluctuation lattice model

Jutta Luettmer-Strathmann,[1,a)] Federica Rampf,[2] Wolfgang Paul,[2] and Kurt Binder[2]

[1]*Department of Physics, University of Akron, Akron, Ohio 44325-4001, USA and Department of Chemistry, University of Akron, Akron, Ohio 44325-4001, USA*

[2]*Institut für Physik, Johannes-Gutenberg-Universität, Staudinger Weg 7, D-55099 Mainz, Germany*

A polymer chain tethered to a surface may be compact or extended, adsorbed or desorbed, depending on interactions with the surface and the surrounding solvent. This leads to a rich phase diagram with a variety of transitions. To investigate these transitions we have performed Monte Carlo simulations of a bond fluctuation model with Wang–Landau and umbrella sampling algorithms in a two-dimensional state space. The simulations' density-of-states results have been evaluated for interaction parameters spanning the range from good- to poor-solvent conditions and from repulsive to strongly attractive surfaces. In this work, we describe the simulation method and present results for the overall phase behavior and for some of the transitions. For adsorption in good solvent, we compare with Metropolis Monte Carlo data for the same model and find good agreement between the results. For the collapse transition, which occurs when the solvent quality changes from good to poor, we consider two situations corresponding to three-dimensional (hard surface) and two-dimensional (very attractive surface) chain conformations, respectively. For the hard surface, we compare tethered chains with free chains and find very similar behavior for both types of chains. For the very attractive surface, we find the two-dimensional chain collapse to be a two-step transition with the same sequence of transitions that is observed for three-dimensional chains: a coil-globule transition that changes the overall chain size is followed by a local rearrangement of chain segments. © *2008 American Institute of Physics*. [DOI: 10.1063/1.2837459]

I. INTRODUCTION

Chain molecules anchored at surfaces are a part of many physical systems. Examples include polymer chains grafted to colloidal particles,[1] proteins projecting from cell membranes,[2] block copolymers at liquid air interfaces,[3,4] and long chain molecules attached to inorganic surfaces for study with atomic force microscopes.[5] Parameters such as composition of the chains, grafting density, and interactions with the surface and the environment affect the properties of these systems by determining the conformations of the chains. In this work we focus on the effects of solvent quality and surface interactions and investigate individual polymer chains tethered to a flat, impenetrable surface. A tethered chain near an attractive surface has many of the conformation characteristics of a free chain adsorbed from solution. Likewise, a tethered chain near a hard surface has much in common with an isolated free chain. These similarities allow us to compare with known results for free chains to validate our approach. They also suggest that our new results are relevant to the process of surface adsorption from dilute polymer solutions.

As is well known, the collapse transition that a flexible polymer chain undergoes in dilute solution when the solvent quality deteriorates is one of the fundamental problems in the statistical mechanics of polymers. It is of crucial importance in understanding the phase diagrams of polymer solutions and still offers surprising insights.[6] Of similar importance is the adsorption transition in good solvent, where the conformations of a tethered chain change from "mushroom" to "pancake" configurations as the strength of the surface-monomer attraction increases. This problem has attracted longstanding intense attention as a basic phenomenon of polymer chains interacting with interfaces.[7] Of course, both "transitions" are sharp thermodynamic phase transitions only in the (thermodynamic) limit when the chain length tends to infinity, but understanding how this limit is precisely approached is one of the challenges here.

In the present work, we go one step beyond the problems outlined above, by considering the interplay of adsorption and collapse. This problem is essential for understanding polymeric aggregates on surfaces when no solvent is present (e.g., adsorbed polymers on a surface exposed to air!). It is also a first step towards the treatment of heteropolymers at surfaces, a system suited to give insight into the behavior of biopolymers at biological interfaces, membranes, etc., since these polymers of biological interest often assume rather dense conformations. However, even the case of a homopolymer at a surface undergoing adsorption competing with collapse is a very difficult problem, and despite earlier numerical studies[8–17] not yet fully understood. In particular, the question how the polymer model may affect the observed phenomena merits further investigation. In most of the existing work, the polymer has been modeled as an interacting self-avoiding walk on a simple cubic lattice (ISAW). In the

a)Electronic mail: jutta@physics.uakron.edu.

ISAW model, the bond length is fixed to the size of the lattice constant and the bond angles are restricted to the values of $\pi/2$ and π. This leads to very specific chain conformations in poor-solvent conditions, where a chain near an attractive surface fills the volume of a rectangular box.[13,14,17] In contrast, an off-lattice model of a polymer chain under such conditions has chain conformations whose shapes resemble the spherical caps that are typical for partially wetting liquid drops.[18] In this work, we employ the bond fluctuation (BF) model to investigate tethered chains. In the BF model, there are five allowed bond lengths leading to a large set of allowed bond angles.[19–21] In terms of chain conformations, the BF model may be considered an intermediate between the ISAW lattice model and coarse-grained off-lattice models such as bead-spring models. In crystallizable homopolymers such as polyethylene and poly(ethylene oxide) the local structure of the chains leads to an alignment of chain sections and lamella formation upon crystallization.[22] The necessity for mesoscopic conformational ordering accompanying this alignment gives rise to a large entropic barrier to crystallization and makes kinetic effects a dominant factor in polymer crystallization. Therefore it is difficult to separate thermodynamic effects from nonequilibrium effects. In coarse-grained models of polymers, such as the BF model and typical bead-spring models, one can choose force fields with sufficient local flexibility to allow for crystallization by local rearrangement of monomers. This reduces the entropic barrier to crystallization and allows the systems to reach ordered equilibrium states. While their lack of lamella formation hampers the comparison with experimental data for simple crystallizable homopolymers, the lower entropic barriers of coarse-grained models allow us to study equilibrium aspects of polymer crystallization. The BF model has proven to be a very useful model for a range of polymeric systems (see, for example, Refs. 19–21 and 23–25) but has not yet been investigated in the present context.

The combined effects of surface interactions and solvent quality lead to a variety of transitions for a polymer chain tethered to a surface. In Fig. 1 we present a schematic phase diagram that represents insights from theoretical and simulation work on lattice models of tethered polymer chains[8–14] including results presented in this work. The field variables β_s and β_b are a combination of inverse temperature and interaction parameters[8,14] and will be defined in Sec. III. The field β_s describes the effect of surface interactions and increases with increasing attraction between the surface and the chain segments. The field β_b describes the net interactions between monomers of a polymer chain in solvent. β_b is small for a chain in a good solvent and increases with decreasing solvent quality, corresponding to increasing net attractive interactions between monomers.

The regions marked DE (desorbed extended) and AE (adsorbed extended) correspond to good-solvent conditions. With field values in the DE region, a tethered chain assumes extended three-dimensional conformations that are often described as mushrooms. An increase of the surface field β_s leads to chain adsorption. For fields in the AE region, the chain conformations are (nearly) two dimensional and extended; they are sometimes called pancake conformations.
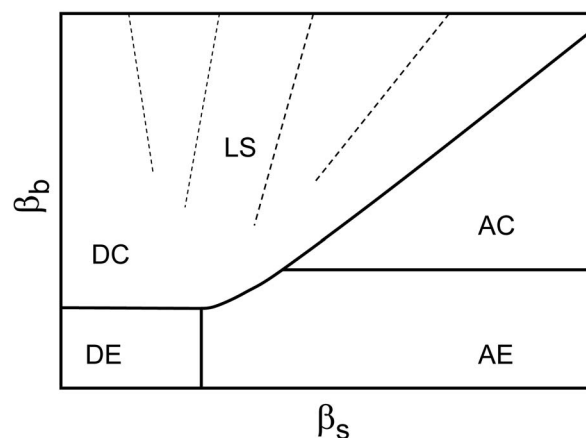

FIG. 1. Schematic phase diagram for tethered chains of finite length in the space of field variables β_b and β_s (see Sec. III for the formal definition). As discussed in the text, increasing values of β_s and β_b correspond to increasingly attractive surface- and monomer-monomer interactions, respectively. The lines indicate transitions between states identified by the following abbreviations: DE for desorbed extended (mushroom), AE for adsorbed extended (pancake), DC for desorbed compact, AC for adsorbed compact, and LS for layered states. The solid lines indicate transitions that are expected to become true phase transitions in the limit of infinite chain length. The dashed lines represent structural transitions observed for finite size chains only. The ending of the dashed lines indicates that, in simulations, these structural transitions can no longer be uniquely identified in regions of field parameters, where several transitions compete with each other.

The transition from DE to AE states has been investigated with theoretical and simulation methods for a variety of models (see, for example, Refs. 18 and 26–29). In the limit of infinite chain length, the adsorption transition is sharp and corresponds to a multicritical point.

The regions marked DC (desorbed compact), AC (adsorbed compact), and LS (layered states) correspond to poor-solvent conditions. Subject to fields in the DC region, a chain assumes compact three-dimensional globule conformations and for fields in the AC region the corresponding two-dimensional conformations. The region labeled LS is characterized by a competition between the effects of attractive surface and monomer interactions.

For weak surface fields β_s, an increase in the field β_b leads to chain collapse, i.e., the coil-globule transition from DE to DC states. For free chains, the coil-globule transition is a continuous transition which may be followed by a first-order transition that is associated with spatial ordering of the chain segments (see, for example, Refs. 30–32). From theoretical work on the ISAW model, the line describing the coil-globule transition is expected to be a straight line parallel to the β_s axis[8] and perpendicular to the adsorption transition line. For strongly attractive surfaces, i.e., for large β_s values, an increase in β_b leads to a transition from AE to AC states. In analogy with the coil-globule transition of a free chain in two dimensions, this transition is expected to be continuous for ISAW models.[9]

Adsorption in poor solvent occurs for high β_b values as the surface field β_s is increased. It takes a tethered chain from desorbed globule conformations in three dimensions (DC) to compact, single-layer conformations (AC) through

intermediate states (LS) that are not yet fully understood and appear to be model dependent. Singh and co-workers [11–13] investigated *untethered* chains by exact enumerations of interacting self-avoiding walks on a simple cubic lattice (ISAW model). In poor-solvent conditions, a free chain assumes its most compact conformation which, in the ISAW model, has the shape of a cube with side length $l \propto N^{1/3}$, where N is the length of the chain. In the presence of a (slightly) attractive surface, the cubic globule attaches itself to the surface and makes a number of surface contacts proportional to the area of a face of the cube, i.e., $\propto N^{2/3}$. Singh and co-workers [11–13] interpret the transition from the detached to the attached globule as a surface transition from the DC phase to a "surface-attached globule" phase, which occupies the LS region in Fig. 1, and is followed by a second phase transition at high β_s values to the AC phase. For *tethered* chains in the ISAW model, theoretical arguments suggest that there is only one true phase transition (nonanalyticity of the free energy in the limit of infinite chain length) as β_s is varied at constant β_b.[8] More recent simulations of tethered chains in the ISAW model by Krawczyk *et al.*[14] found the chains to undergo a series of layering transformations in the LS region corresponding to transitions between compact chain conformations with different numbers of layers parallel to the surface. This work identified scaling relations which suggest that, with increasing chain length, the transitions become sharper and more numerous, and that the transitions merge into a single transition in the limit of infinite chain length. In the diagram of Fig. 1, we represent the true phase transition by a solid line between the AC and LS regions. The dashed lines in Fig. 1 indicate structural/layering transitions that may not become phase transitions in the infinite chain limit. These transitions are important, however, since for many problems the behavior of finite-length chains is of physical interest.

In this work, we investigate transitions of tethered polymer chains with the aid of density-of-states simulations of a bond fluctuation model. In the work presented here we focus on characteristic features of adsorption in good solvent (DE to AE) and chain collapse in two and three dimensions (DE to DC and AE to AC). We also construct a phase portrait for our longest chain. In a forthcoming publication we shall discuss adsorption in poor solvent and investigate some states and transitions in detail. In this article, we introduce the bond fluctuation model for a tethered chain and describe the simulation methods in Sec. II and the data evaluation in Sec. III. Results of our simulations are presented and discussed in Sec. IV, followed by a brief summary and conclusions in Sec. V. Technical details of the simulations undertaken for this work are presented in the Appendix.

II. MODEL AND SIMULATION METHOD

In this section, we present the model for a surface-attached polymer chain and the simulation methods employed in this work. Details of the simulation protocol that are of interest to those who want to reproduce or extend the work but that are not required for an understanding of the following sections have been relegated to the Appendix.

In the BF model,[19–21] monomers of a polymer chain occupy sites on a simple cubic lattice. The bond lengths between monomers are allowed to vary between $b=2a$ and $b=\sqrt{10}a$, where a is the lattice constant, which we set to unity, $a=1$. A tethered chain is represented by a chain whose first monomer is fixed just above a hard surface. The position of the surface is the x-y plane at position $z=0$ in a Cartesian coordinate system; the coordinates of the fixed monomer are $(1,1,1)$. Monomers at $z=1$ are considered to be in contact with the surface and contribute an amount ϵ_s to the energy. The interactions between monomers depend on the distance. A pair of monomers i and j at a distance r_{ij} contributes an amount of ϵ_b to the energy when $4 \le r_{ij}^2 \le 6$. Distances $r_{ij}^2 < 4$ are prohibited by hard core repulsion, while monomers do not interact for $r_{ij}^2 > 6$. The total energy of the system is given by

$$E(n_s, n_b) = n_s \epsilon_s + n_b \epsilon_b, \tag{1}$$

where n_s and n_b are the number of monomer-surface and monomer-monomer contacts, respectively. We refer to a pair of contact numbers, (n_s, n_b), as a state of the system.

In the Monte Carlo simulations described here, two types of elementary moves were carried out; local moves that displace a monomer to a nearest neighbor lattice site and pivot moves about the z-axis. Simulations were performed for chains of length $N=16$, $N=32$, and $N=64$. In all simulations, N local move attempts were followed by ten pivot move attempts. We refer to this sequence as one Monte Carlo (MC) step.

A. Wang–Landau algorithm for a two-dimensional state space

The density of states (DOS), $g(n_s, n_b)$ is the number of configurations for a given state (n_s, n_b) of the system. The Wang–Landau (WL) algorithm[33,34] is an iterative Monte Carlo simulation method for constructing the density of states. Originally formulated for a one-dimensional state space, characterized by the total energy, it has been extended to state spaces of higher dimensions.[35–37] In this work, the state space is the two-dimensional space of contact numbers n_s and n_b.

In the WL algorithm, an elementary move attempt from a state (n_s, n_b) to a state (n_s', n_b') is accepted with probability

$$p((n_s, n_b) \rightarrow (n_s', n_b')) = \min\left(\frac{g(n_s, n_b)}{g(n_s', n_b')}, 1\right), \tag{2}$$

where $g(n_s, n_b)$ is the current estimate for the density of states.

The initial guess for the density of states is $g(n_s, n_b)=1$ for all states (n_s, n_b). At each iteration level, elementary move attempts are followed by an update of the density of states and the histogram of visits to the states, $h(n_s, n_b)$. After an attempted move from a state (n_s, n_b) to a state (n_s', n_b') the updates are given by

$$\text{if accepted:} \begin{cases} \ln(g(n_s', n_b')) & \rightarrow & \ln(g(n_s', n_b')) + \ln(f) \\ h(n_s', n_b') & \rightarrow & h(n_s', n_b') + 1, \end{cases}$$
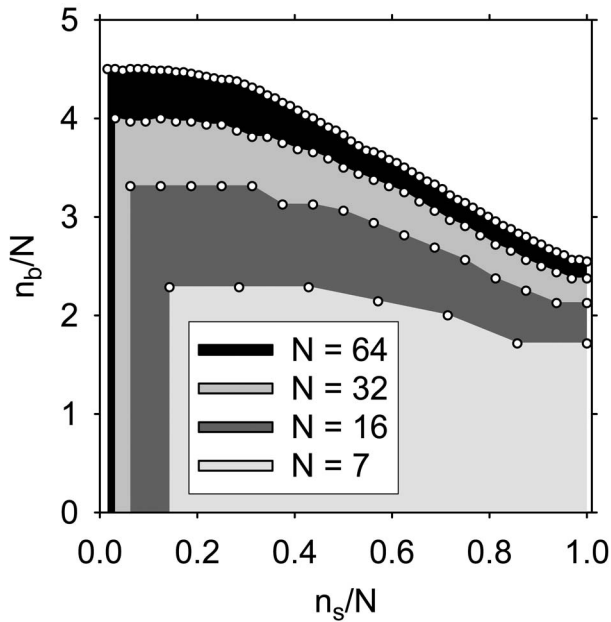
$$\tag{3}$$

FIG. 2. Ranges of accessible states for tethered chains of lengths $N=7$, 16, 32, and 64. The shaded areas approximate the ranges, and the symbols represent the realized states with the highest number of bead contacts n_b for a given number of surface contacts n_s. The results for $N=7$ were obtained in exact enumeration.

$$\text{if rejected:} \begin{cases} \ln(g(n_s,n_b)) & \rightarrow & \ln(g(n_s,n_b)) + \ln(f) \\ h(n_s,n_b) & \rightarrow & h(n_s,n_b) + 1, \end{cases}$$

$$(4)$$

where f, with $f>1$, is the refinement factor. An iteration is considered complete when the histogram satisfies a flatness criterion. In a typical Wang–Landau simulation,[33,34] a histogram is considered flat when the smallest value in the histogram is at least 80% of the average value of the histogram entries. At that point, the histogram is reset to 0 for all states and the refinement factor is reduced before the next iteration is started. The adjustments to the density of states become smaller with each iteration level; we used refinement levels with $\ln(f_k)=2^{-(k-1)}$ for $k \in \{2,20\}$.

For tethered chains, the range of accessible states (n_s,n_b) is not known *a priori*. Since the maximum number of surface contacts n_s is equal to the number of monomers N, the maximum value of the ratio n_s/N is unity for all chain lengths. However, the maximum value of n_b/N, the number of monomer-monomer contacts per monomer, increases with chain length as illustrated in Fig. 2. In addition, for each chain length, the maximum number of monomer-monomer contacts decreases with increasing number of surface contacts. In the work presented here, we allow the range of considered states to change during the simulations. During the Wang–Landau simulations, when a configuration to a previously unvisited state (n'_b,n'_s) appears, the new state is assigned the initial DOS value $g(n'_s,n'_b)=1$ and the move is accepted or rejected with the usual criterion.

For simulations of free chains in the bond fluctuation model, it was found that updating after accepted moves only may lead to shorter simulation times without affecting the results for the density of states.[38] In the work presented here,

we carried out simulations where either both updates, Eqs. (3) and (4), or only the updates after accepted moves, Eq. (3), were carried out.

B. Multiple replica algorithm

In a multiple replica simulation, the state space is divided into a number of overlapping regions. Standard simulation steps are carried out separately in each replica. After each MC step, an attempt is made to exchange the chains of two neighboring replicas if their configurations belong to states in the overlap region of the replicas. The acceptance criterion for such a replica-swapping move is

$$p([(n_s,n_b)_i,(n'_s,n'_b)_{i+1}] \rightarrow (n'_s,n'_b)_i,(n_s,n_b)_{i+1}])$$

$$= \min\left(\frac{g(n_s,n_b)_{i+1}}{g(n'_s,n'_b)_i} \frac{g(n'_s,n'_b)_{i+1}}{g(n_s,n_b)_i}, 1 \right), \quad (5)$$

where i and $i+1$ are the indices for neighboring replicas. When using the method to generate the density of states, the DOS values are updated after each attempted move in the usual way, see Eqs. (3) and (4). The density of states for the whole state space is obtained at the end of the simulation by combining the results for each replica. For the results presented here, we used regions that were defined by intervals in the number of bead-bead contacts n_b and contained all possible surface contacts. We experimented with regions of different sizes and different ranges of overlap and found that small but systematic errors in the density of states occurred unless each state was covered by the same number of replicas. We worked with a total of three to five overlapping replicas covering each region with two replicas.

C. Global update algorithm

When the WL algorithm is applied to large two-dimensional state spaces much time is spent accumulating the large $\ln(g)$ values belonging to the interior of the state space. Introducing global updates[35] improves the efficiency by allowing the simulation to spend more time exploring the edges of the current state space. In a global update algorithm, a simulation is started at a given refinement level and the current values of $\ln(g(n_s,n_b))$ are compared with a threshold value ω. Once density-of-states values above the threshold, $\ln(g(n_s,n_b)) > \omega$, are found, they are augmented in the following way:

$$\ln(g) \rightarrow \ln(g) + \kappa \exp\left(\frac{-\lambda}{\ln(g) - \omega} \right) \Theta(\ln(g) - \omega), \quad (6)$$

where Θ is the Heaviside step function. The exponential function dampens the shift from a maximum value of κ for states with $\ln(g)$ values well above the threshold to zero for states at the threshold; the parameter λ determines the range over which the shift is phased out. The simulation then continues with standard steps and local updates to the density of states. Immediately after a global shift, states that were outside the shifted region are preferentially sampled. With time, their $\ln(g)$ values increase thereby decreasing the acceptance rates for moves to those states and leading to uniform sampling over previously shifted and unshifted states. Once uni-

form growth over the current state space has resumed the next global update is considered. This continues until a flatness criterion is satisfied or the simulation is terminated by hand.

To determine when uniform growth has been achieved in our simulations, we monitor the difference $\Delta \ln(g)$ between the current value of the log-density of states and that at the time of the global shift. When for each previously shifted state the difference $\Delta \ln(g)$ is larger than a fixed parameter ρ, we conclude that uniform growth has been achieved. We found that the values for the parameters κ, λ, ω, and ρ can have a large effect on the quality of the results. In particular, systematic deviations in the results for the density of states occur when the global updates are too large and occur too frequently.

D. Umbrella sampling

In multicanonical or umbrella sampling simulations with single histogram reweighing, a good estimate for the density of states $g(n_s,n_b)$ is required as input (see, for example, Refs. 21 and 39–41). We performed umbrella sampling simulations with a WL result as the initial DOS for all simulation results reported here. During the simulation, elementary moves are accepted with the usual criterion, see Eq. (2), and the histogram is updated after accepted and rejected moves. The DOS values, however, are updated only at the end of the simulations. In a typical single histogram reweighing step, the logarithm of the final histogram entry $h(n_s,n_b,t_f)$ is added to the original log-density of states values,

$$\ln(g'(n_s,n_b)) = \ln(g(n_s,n_b)) + \ln(h(n_s,n_b,t_f)). \tag{7}$$

In the work presented here, we record cumulative histograms at regular intervals, determine the slope $m(n_s,n_b)$ of the histogram entries as a function of time, and estimate the final histogram entry from the slope $h(n_s,n_b,t_f) \simeq m(n_s,n_b)t_f$. This gives a slightly more reliable DOS estimate for states that are not visited in every block.

E. Metropolis algorithm

For comparison with results from the density-of-states algorithms and in order to sample efficiently some parts of phase space during the production stage, some simulations were performed with a Metropolis acceptance criterion at fixed fields β_s and β_b. The probability for accepting a move from a state (n_s,n_b) to a state (n'_s,n'_b) in the Metropolis algorithm may be written as

$$p((n_s,n_b) \rightarrow (n'_s,n'_b))$$
$$= \min(\exp[\beta_s(n'_s - n_s) + \beta_b(n'_b - n_b)],1). \tag{8}$$

F. Production stage

In a production simulation, chain conformations are evaluated at regular intervals to accumulate configurational properties as a function of the pairs of contact numbers (n_s,n_b). We determined a range of configurational properties including chain dimensions and density profiles. Furthermore, configurations were stored for a detailed analysis of the chain structure. In this work, we present results for the squared bond length $B^2 = \Sigma_i(\mathbf{r}_{i+1}-\mathbf{r}_i)^2/(N-1)$, where $\mathbf{r}_i$ is the position vector of monomer i, and for the radius of gyration R_g. In order to investigate the effect of the surface, we calculate parallel and perpendicular contributions to R_g^2 according to

$$R_{g,z}^2 = \frac{1}{N^2}\sum_{i<j}(z_i - z_j)^2, \tag{9}$$

$$R_{g,xy}^2 = \frac{1}{N^2}\sum_{i<j}[(x_i - x_j)^2 + (y_i - y_j)^2], \tag{10}$$

where $i,j \in \{1,\ldots,N\}$ and where x_i,y_i,z_i are the Cartesian coordinates of monomer i, and $R_g^2 = R_{g,z}^2 + R_{g,xy}^2$.

When production simulations are performed with the acceptance criterion of the Wang–Landau algorithm all states (n_s,n_b) are visited approximately equal numbers of times. This may lead to insufficient sampling of states (n_s,n_b) with a diverse set of chain conformations. In order to improve the statistics for the configurational properties belonging to such states (n_s,n_b), we performed additional production simulations with a Metropolis Monte Carlo algorithm for fields between $\beta_s=\beta_b=0$ and $\beta_s=\beta_b=-2$. In these simulations, the visitation histograms are approximately Gaussian with maxima at the most probable states for these fields.

For all chain lengths, we performed more than one type of production simulation. During production, block averages[21,42] were calculated and the statistical uncertainty of an average value was determined from the standard deviation of the block averages. Results from different production simulations were combined as weighted averages, where the weights were based on the uncertainty estimates obtained for each quantity in the individual production simulations.

III. EVALUATION OF THE DENSITY OF STATES

The canonical partition function for a tethered chain is given by

$$Z = \sum_{n_s,n_b} g(n_s,n_b)e^{-\beta E(n_s,n_b)}, \tag{11}$$

where $\beta = 1/k_BT$, T is the temperature, k_B is Boltzmann's constant, and $g(n_s,n_b)$ is the density of states. The energy of the state, $E(n_s,n_b)=n_s\epsilon_s+n_b\epsilon_b$, depends on the contact numbers n_s and n_b and the interaction parameters ϵ_s and ϵ_b. In this work, we employ combinations of the interaction parameters and the inverse temperature as field variables[8,14]

$$\beta_s = -\epsilon_s\beta, \quad \beta_b = -\epsilon_b\beta, \tag{12}$$

and write the partition function as

$$Z(\beta_s,\beta_b) = \sum_{n_s,n_b} g(n_s,n_b)e^{\beta_s n_s}e^{\beta_b n_b}. \tag{13}$$

For fixed fields β_s and β_b, the probability $P(n_s,n_b;\beta_s,\beta_b)$ for states with contact numbers (n_s,n_b) is given by

$$P(n_s, n_b; \beta_s, \beta_b) = \frac{1}{Z} g(n_s, n_b) e^{\beta_s n_s} e^{\beta_b n_b}, \qquad (14)$$

and the average values of quantities $Q(n_s, n_b)$ at given fields β_s and β_b are calculated from

$$\langle Q \rangle = \sum_{n_s, n_b} Q(n_s, n_b) P(n_s, n_b; \beta_s, \beta_b) \equiv Q(\beta_s, \beta_b). \qquad (15)$$

At the end of this section, we describe how we estimate uncertainties for the averages determined in this way.

With the definition of a free energy

$$G(\beta_s, \beta_b) = -\ln(Z), \qquad (16)$$

the average number of surface contacts $\langle n_s \rangle$ and the average number of monomer contacts $\langle n_b \rangle$ are conjugate to the field variables β_s and β_b, respectively,

$$\langle n_s \rangle = -\left(\frac{\partial G}{\partial \beta_s} \right)_{\beta_b}, \qquad (17)$$

$$\langle n_b \rangle = -\left(\frac{\partial G}{\partial \beta_b} \right)_{\beta_s}. \qquad (18)$$

The second derivatives of the free energy with respect to the fields define susceptibilities $\chi_{\mu\nu}$, $\mu, \nu \in \{s, b\}$ that are related to the fluctuations in the number of surface and monomer contacts

$$\chi_{ss} = -\left(\frac{\partial^2 G}{\partial \beta_s^2} \right)_{\beta_b} = \langle n_s^2 \rangle - \langle n_s \rangle^2, \qquad (19)$$

$$\chi_{bb} = -\left(\frac{\partial^2 G}{\partial \beta_b^2} \right)_{\beta_s} = \langle n_b^2 \rangle - \langle n_b \rangle^2, \qquad (20)$$

$$\chi_{sb} = -\left(\frac{\partial^2 G}{\partial \beta_s \beta_b} \right) = \langle n_s n_b \rangle - \langle n_s \rangle \langle n_b \rangle. \qquad (21)$$

In terms of these susceptibilities, the heat capacity of the system is given by

$$C = \beta^2 (\langle E^2 \rangle - \langle E \rangle^2) = \beta_s^2 \chi_{ss} + \beta_b^2 \chi_{bb} + 2\beta_s \beta_b \chi_{sb}. \qquad (22)$$

There are alternative methods to evaluate the density of states which we would like to discuss briefly. The density of states $g(n_s, n_b)$ provides the entropy as a function of the contact values up to an arbitrary constant S_0 as follows:

$$S(n_s, n_b) = k_B \ln(g(n_s, n_b)) + S_0. \qquad (23)$$

Starting from the entropy as the thermodynamic potential, the fields and susceptibilities may be expressed in terms of derivatives of the log-density of states. For example, the fields may be obtained as $\beta_s(n_s, n_b) = -(\partial \ln(g)/\partial n_s)_{n_b}$ and $\beta_b(n_s, n_b) = -(\partial \ln(g)/\partial n_b)_{n_s}$. In the thermodynamic limit, $N \to \infty$, results from different statistical ensembles are equivalent; however, for our chain lengths finite size effects may play a role. Since an evaluation of the entropy is hampered by the need to take numerical derivatives of discrete variables, we employ the free energy $G(\beta_s, \beta_b)$ unless otherwise indicated.

In some cases, it is convenient to work with a thermodynamic potential that is a function of the number of surface contacts n_s and the bead-contact field β_b. This free energy $A(n_s, \beta_b)$ may be considered a Legendre transform[43] of either the entropy S or the free energy G and may be written as $A(n_s, \beta_b) = -\ln(Z_A)$, with

$$Z_A(n_s, \beta_b) = \sum_{n_b} g(n_s, n_b) e^{\beta_b n_b}. \qquad (24)$$

In this case, the probability for a state with n_b bead contacts is given by

$$P(n_b; n_s, \beta_b) = \frac{1}{Z_A} g(n_s, n_b) e^{\beta_b n_b}, \qquad (25)$$

which allows us to calculate quantities for given n_s and β_b without taking numerical derivatives. For example, the average number of bead contacts is determined from

$$\langle n_b(n_s, \beta_b) \rangle = \sum_{n_b} n_b P(n_b; n_s, \beta_b). \qquad (26)$$

In general, there are two sources of error when average quantities $\langle Q \rangle = Q(\beta_s, \beta_b)$ for given field values β_s and β_b are obtained from the contact number dependent values $Q(n_s, n_b)$ with the aid of Eq. (15). The first source of error is the uncertainty in the density of states; this is the only uncertainty for quantities such as the susceptibilities, see Eqs. (19)–(21). To estimate this uncertainty, we perform several simulations for the same chain length and calculate the mean value $\overline{\ln(g(n_s, n_b))}$ and the standard deviation $\sigma_{\ln(g)}(n_s, n_b)$ for each state (n_s, n_b). The second source of error is the uncertainty in production results, which we obtain from block averages. For properties such as the chain dimensions, see Eqs. (9) and (10), this is typically the larger source of error.

In order to estimate the effect of the uncertainties in the density of states on calculated properties Q, we generate five synthetic densities of states $\ln(g_i)$ by drawing randomly from Gaussian distributions centered on $\overline{\ln(g(n_s, n_b))}$ with standard deviation $\sigma_{\ln(g)}(n_s, n_b)$ for each state (n_s, n_b). Average values $\langle Q \rangle_i$ are calculated from each synthetic density of states i and the mean $\bar{Q}$ and standard deviations $\sigma_{Q,g}$ of the results are determined. The uncertainties of production data are propagated through Eq. (15), evaluated with $\overline{\ln(g)}$, to obtain the second contribution to the uncertainty $\sigma_{Q,p}$. The combined uncertainty is estimated from $\sigma_Q = \sqrt{\sigma_{Q,g}^2 + \sigma_{Q,p}^2}$.

The uncertainty estimates, $\sigma_{Q,g}$ for results that derive their errors only from the density of states and σ_Q for results that involve production data, are shown as error bars in the figures of this work. Error bars are omitted when they are smaller than the symbol size or the line thickness.

IV. RESULTS AND DISCUSSION

A. Density of states

Density-of-states results were obtained for chains of length $N=16$, $N=32$, and $N=64$ with the simulations described in Sec. II. Figure 2 shows the ranges of accessible states for these chains and also includes results from an exact enumeration for chains of length $N=7$. In each case, the
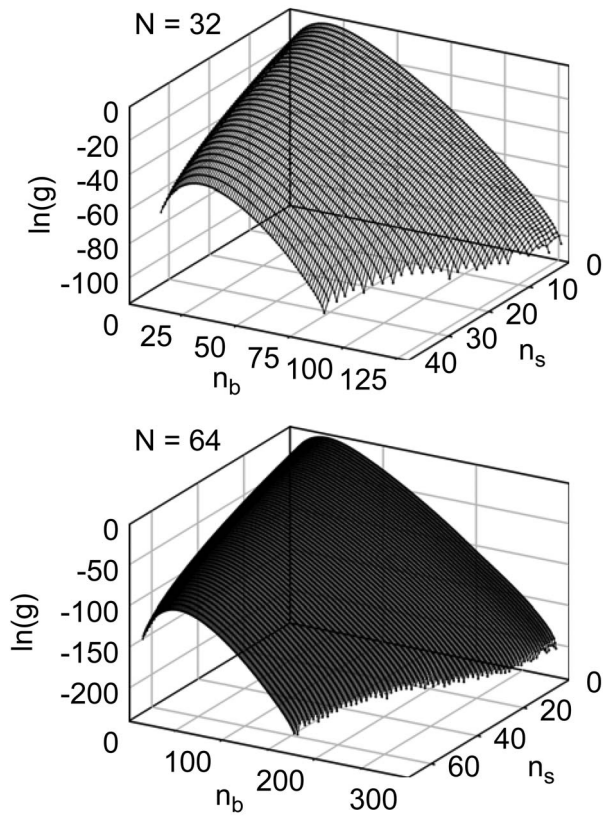
FIG. 3. Density of states for tethered chains of length $N=32$ (top) and $N=64$ (bottom). The surfaces (small symbols connected by straight line segments) represent the log-density of states values, $\ln(g)$, as a function of surface contacts, n_s, and bead-bead contacts, n_b.

TABLE I. Umbrella sampling parameters and some density-of-states characteristics for chains of length $N=16$, $N=32$, and $N=64$. N_u is the number of results for which umbrella sampling simulations were performed, K_u is the length of the simulations in Monte Carlo steps, N_s is the number of states sampled, and $n_{b,\max}(1)$ and $n_{b,\max}(N)$ represent the largest number of bead-bead contacts for $n_s=1$ and $n_s=N$ surface contacts, respectively. The values for the range of the log-density of states ($\Delta \ln(g)$), and its uncertainties ($\sigma_{\ln(g)}$) represent results after umbrella sampling. For $N=16$ and $N=32$, the states in this table are believed to be the complete set; for $N=64$, only states included in our evaluation are represented.

N	16	32	64
N_u	4	3	2
$K_u/10^9$	1	16, 10, 18	18.5, 18.8
N_s	748	3467	15 268
$n_{b,\max}(1)$	53	128	288
$n_{b,\max}(N)$	34	76	163
$\Delta \ln(g)$	50.8	109.5	227
Average $\sigma_{\ln(g)}$	0.008	0.008	0.015
Median $\sigma_{\ln(g)}$	0.004	0.003	0.004
Maximum $\sigma_{\ln(g)}$	0.18	0.5	1.5000

maximum number of bead-bead contacts decreases with increasing number of surface contacts since chain conformations cannot maximize surface and bead contacts simultaneously. This leads to a competition between bead and surface contacts at high field values which increases with increasing chain length.

In Fig. 3 we present results for the log-density of states for chains of length $N=32$ and $N=64$ (the results for $N=16$ show the same qualitative behavior); some characteristic numerical values are presented in Table I. For each surface-contact value, n_s, and for small contact values n_b, the density of states increases with n_b. As n_b increases further, $\ln(g)$ passes through a maximum and then decreases with increasing n_b. As discussed at the end of Sec. III, the slope of $\ln(g(n_s,n_b))$ at fixed n_s is related to the expectation value of the field $\beta_b(n_s,n_b)$. This suggests that states with small bead-contact values are predominantly populated for negative β_b fields (repulsive interactions between the beads) while states with large bead-contact values are populated for positive β_b fields (attractive bead-bead interactions). This is confirmed by an evaluation of the average bead-contact number according to Eq. (26). In Fig. 4 we present results for the average number of bead contacts $\langle n_b(n_s,\beta_b)\rangle$ as function of the number of surface contacts for five fields β_b. For each n_s and β_b we also evaluated cumulative probabilities $\sum_{n_b=0}^{n*_b} P(n_s,\beta_b;n_b)$ and determined the bead-contact numbers $n*_{b,1}$ and $n*_{b,2}$ where the cumulative probability first exceeds $1/6$ and $5/6$,

respectively. The states between $n*_{b,1}$ and $n*_{b,2}$ have significant probability of occupation and are indicated by the shaded areas in Fig. 4. As expected, the range of significantly populated states shifts from low-n_b to high-n_b values with increasing field β_b. For the largest field shown, $\beta_b=2$, states on the upper rim of the range of accessible states start to become populated. Since the density-of-states values for rim states have a relatively large uncertainty, we restrict ourselves in this work to fields $\beta_b \leq 2$. The width of the shaded areas in Fig. 4 is an indication for the size of the fluctuations about the mean value. These fluctuations are larger for β_b
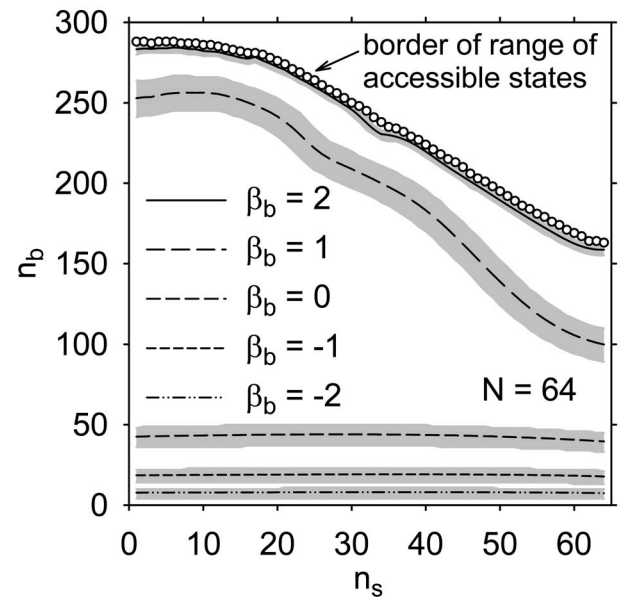

FIG. 4. Most probable states for a given number of surface contacts n_s and field β_b. The lines represent the average number of bead contacts $\langle n_b(n_s,\beta_b)\rangle$ as function of the number of surface contacts for five fields β_b, as indicated in the figure. The shaded areas surrounding the lines indicate the states that have significant probability of occupation; the sum of the probabilities associated with these states is $2/3$. The symbols at the upper boundary of the graph indicate the maximum values of n_b for given n_s.
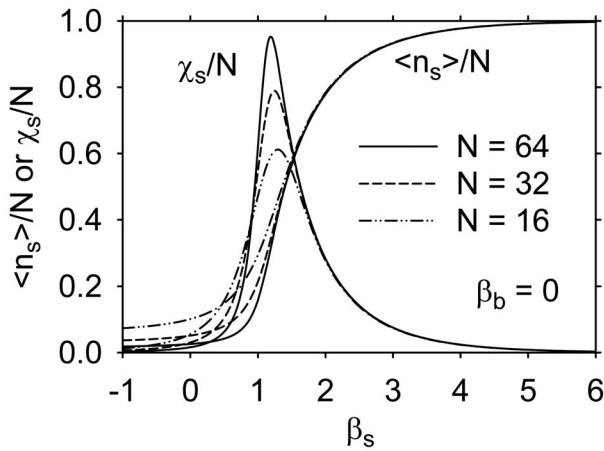
FIG. 5. Average number of surface contacts per monomer $\langle n_s \rangle / N$ and surface-contact fluctuations χ_s / N, as a function of the surface field β_s for good-solvent conditions ($\beta_b=0$). The lines represent results from the evaluation of the density of states for chains of length $N=64$ (solid), 32 (dashed), and 16 (dash dotted), respectively. The graphs for $\langle n_s \rangle / N$ are monotonously increasing; those for χ_s / N have a maximum in the transition region.
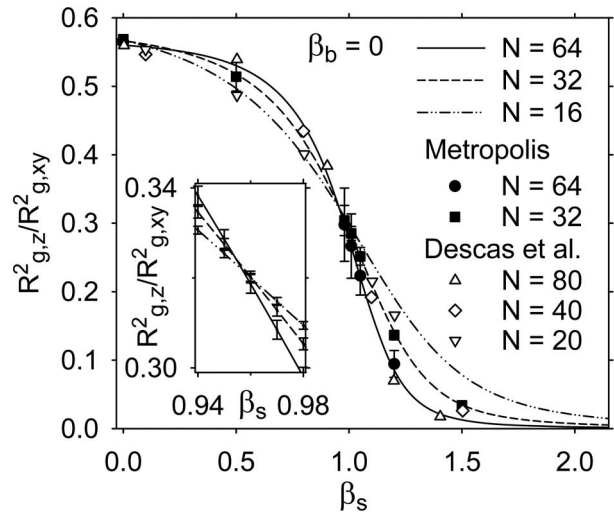

FIG. 6. Ratio $R_{g,z}^2 / R_{g,xy}^2$ of perpendicular and parallel contributions to the square radius of gyration as a function of the surface field β_s for good-solvent conditions ($\beta_b=0$). The lines represent results from the evaluation of the density of states and production data for chains of length $N=64$ (solid), 32 (dashed), and 16 (dash dotted); the inset shows an enlargement of the region where the lines cross. For clarity, error bars for our calculated values are shown only in the inset. (The error bars generally increase with increasing N and decreasing β_s; for $\beta_s=0$ they are about twice as large as for the β_s-range of the inset). The filled symbols with error bars represent Metropolis Monte Carlo results from this work. The open symbols represent Metropolis Monte Carlo results for chains of length $N=20$, 40, and 80 by Descas *et al.* (Ref. 29).

$=1$ than for the other fields, since $\beta_b=1$ is closer to the field value of the coil-globule transition (see Sec. IV C) than the others. Geometrically, the size of the fluctuations is associated with the inverse of the curvature of the log-density of states surface.

For most accessible states, the density of states is a monotonously decreasing function of n_s at constant n_b, i.e., the states are predominantly occupied for attractive surface interactions. Only for a range of states with small n_s and very large n_b values is the slope of $\ln(g)$ for fixed n_b positive. These states become populated predominantly when β_s is negative and β_b is large and positive.

B. Adsorption in good solvent

To explore adsorption in good-solvent conditions, the bead-contact field is set to $\beta_b=0$ so that chain segments interact with each other only through excluded volume interactions. Density of states and production results are evaluated as described in Sec. III for a range of surface fields β_s. In Fig. 5 we present results for the average number of surface contacts and their fluctuations as a function of the surface field β_s. For negative β_s values, the surface is repulsive and the number of surface contacts is near 1, the smallest possible value. As β_s increases, the surface becomes increasingly more attractive and the number of surface contacts increases until it approaches N, the largest possible value. The transition between desorbed and adsorbed states becomes steeper with increasing chain length which is an expected finite size effect. The fluctuations χ_s are small for repulsive and very attractive surfaces and have a maximum in the transition region. The locations of the maxima are $\beta_s=1.29$, 1.24, and 1.19 for chains of length $N=16$, 32, and 64, respectively. We use maxima in χ_s to identify the transition fields for surface adsorption in Sec. IV E.

The shape of a tethered chain may be described with the contributions $R_{g,z}^2 \equiv R_{g,\perp}^2$ and $R_{g,xy}^2 \equiv 2R_{g,\parallel}^2$ to the radius of gyration R_g^2.[26] For repulsive or weakly adsorbing surfaces,

the chain assumes mushroom configurations whose extensions parallel and perpendicular to the wall are comparable, $R_{g,\perp} \gtrsim R_{g,\parallel}$. As the surface becomes more attractive, $R_{g,\perp}$ decreases and $R_{g,\parallel}$ increases, so that the ratio $R_{g,z}^2 / R_{g,xy}^2 = 0.5 R_{g,\perp}^2 / R_{g,\parallel}^2$ decreases rapidly in the transition region. A scaling analysis shows that the ratio is independent of chain length at the adsorption transition.[26] In Fig. 6 we present results for the ratio $R_{g,z}^2 / R_{g,xy}^2$ as a function of β_s for $\beta_b=0$. The lines represent results from an evaluation of our density of states and production results for chains of length $N=16$, 32, and 64. For comparison, we have also included Metropolis Monte Carlo results obtained by us for chains of length $N=32$ and 64, and by Descas *et al.*[29] for chains of length $N=20$, 40, and 80. The agreement between data obtained with different methods is good. While longer chains are required for a detailed comparison with scaling predictions, our results for $R_{g,z}^2 / R_{g,xy}^2$ show reasonable behavior. The lines for $N=64$, 32, and 16 intersect each other at about $\beta_s=0.96$, as shown in the inset. Our value for the intercept, $\beta_s=0.96 \pm 0.02$, is consistent with the results of Descas *et al.*,[29] who determined an intercept of $\beta_s=0.98 \pm 0.03$ from data which included chains up to length 200.

C. Chain collapse for a hard surface

A polymer chain undergoes a transition from extended to compact conformations, the coil-globule transition, when the solvent quality changes from good to poor. For the bond fluctuation model with attractive bead-bead interactions, $\epsilon_b < 0$, this transition may be induced by reducing the temperature. The continuous coil-globule transition is followed by a
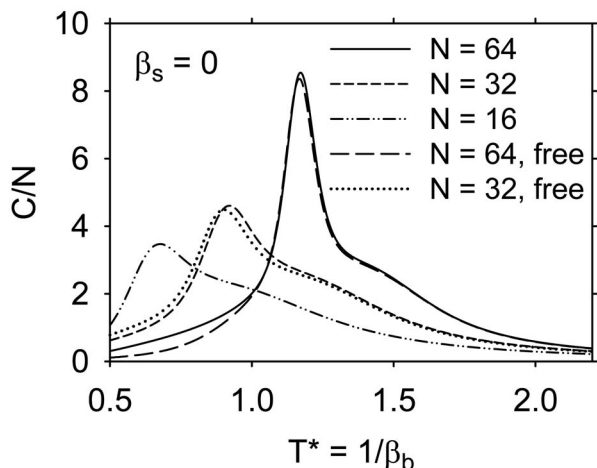
FIG. 7. Heat capacities per monomer, C/N, as a function of the reduced temperature $T^* = 1/\beta_b$. The solid ($N=64$), short-dashed ($N=32$), and dash-dotted ($N=16$) lines represent results for chains tethered to a hard surface ($\beta_s=0$). The long-dashed ($N=64$) and dotted ($N=32$) lines represent results for free chains (Refs. 32 and 38). The estimated uncertainties of the results for the tethered chains are smaller than the line thickness, except for $N=64$ at very low temperatures, $T^* < 0.7$, where they correspond to about twice the line thickness.

FIG. 8. Monomer-monomer contact fluctuations, χ_b/N, as a function of the field β_b for a hard surface, $\beta_s=0$. The lines represent results from the evaluation of the density of states for tethered chains of length $N=64$ (solid), 32 (dashed), and 16 (dash dotted).

discontinuous crystallization transition at lower temperature. For the model we are studying, which has a range of attractive interaction $\leq \sqrt{6}$, the difference between the transition temperatures decreases with chain length and, in the limit $N \to \infty$, the transitions merge into a single first-order transition.[32]

To explore chain collapse for tethered chains, we consider first a hard surface and set $\beta_s=0$. In Fig. 7 we present results for the heat capacity, C, as a function of the reduced temperature $T^* = 1.0/\beta_b$ obtained by evaluating our density of states results for chains of length $N=16$, 32, and 64. For comparison, we also present results for the heat capacity of free chains of length $N=32$ and $N=64$, obtained from Wang–Landau simulations of the BF model.[32,38] For each chain length considered here, the heat capacity shows a peak at low temperatures followed by a shoulder at higher temperatures. For free chains, the peak is associated with the crystallization transition and the shoulder marks the coil-globule transition; we find the same to be true for the tethered chains. In Fig. 11(a) we present an example for a compact and highly ordered conformation of a chain of length $N=64$ that is typical for the lowest temperatures.

While the heat capacity values for the tethered and free chains coincide at high temperatures, there are some differences at lower temperatures. For chains of length $N=64$ and temperatures smaller than $T^* \approx 1$, the free chain heat capacity values are lower than those of the tethered chain. This is due to a difference in the simulations; for the free chain, a cutoff of 272 bead contacts was used while the tethered chain results include bead contacts up to $n_{b,max}=288$. For somewhat higher temperatures, $1 \lesssim T^* \lesssim 1.5$, there is also a small temperature shift (barely visible in the graph) between the heat capacity curves of the free and tethered $N=64$ chains. For chains of length $N=32$ and temperatures smaller than about $T^*=1.2$, i.e., below the coil-globule transition, the heat ca-
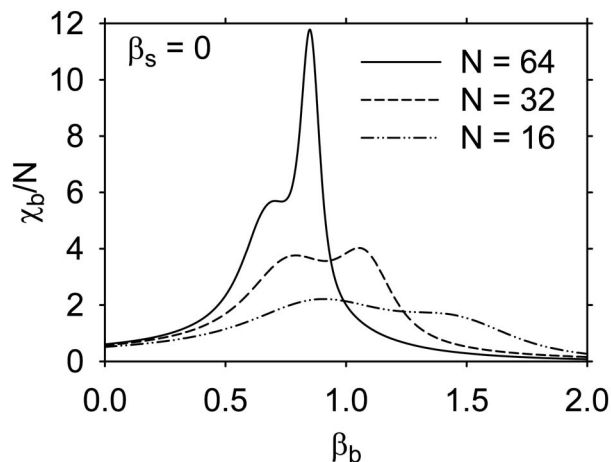
pacity curve for the free chain is shifted to lower temperatures compared to that of the tethered chain. A comparison of the normalized density-of-states results for the free and tethered chains of length $N=32$ shows that the number of available conformations decreases with increasing bead-contact number more rapidly for free chains than for tethered chains. This suggests that the hard surface reduces the relative number of extended conformations more than the relative number of compact conformations. Since the fraction of monomers belonging to the surface of a conformation decreases with chain length, it seems reasonable that the effect is larger for shorter chains; in our simulations, the effect has all but disappeared for $N=64$. In the limit $N \to \infty$, we expect the transition temperature for the three-dimensional coil-globule transition to be the same for free and tethered chains.

To determine the location of the transitions it is convenient to consider the fluctuations in the number of bead contacts χ_b. These are related to the heat capacity through Eq. (22). In Fig. 8 we present tethered chain results for χ_b as function of the field β_b for chains of length $N=16$, 32, and 64 at $\beta_s=0$. The graphs for $N=32$ and $N=64$ show two well separated maxima while the graph for $N=16$ has one maximum associated with the coil-globule transition and a shoulder associated with the globule-globule transition. The locations of the maxima for the coil-globule transitions are 0.91, 0.79, and 0.71 for chains of length $N=16$, 32, and 64, respectively. The field values for the globule-globule transitions are 1.47 (estimated), 1.05, and 0.850 for $N=16$, 32, and 64 respectively. The values for the globule-globule transitions compare well with those obtained from the peaks in the heat capacity, which yield β_b values of 1.48, 1.08, and 0.853 for $N=16$, 32, and 64, respectively. We use maxima in χ_b to identify the transition fields for chain collapse in Sec. IV E.

The transitions of single untethered polymer chains have been investigated intensively with a variety of off-lattice polymer models.[30,31,44–51] Except for the shortest chains and the most short-ranged interactions, the heat capacity as a function of temperature shows two prominent features; a
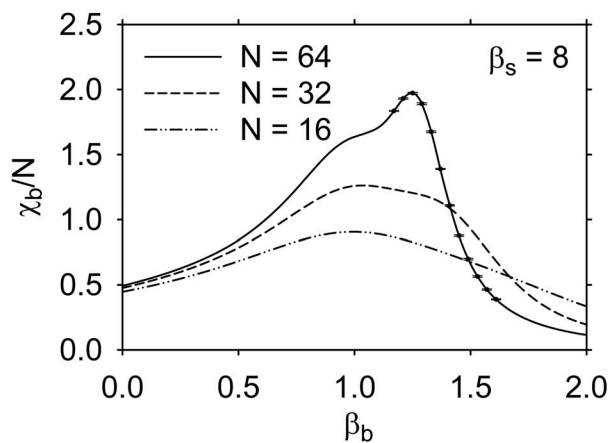
FIG. 9. Monomer-monomer contact fluctuations, χ_b/N, as a function of the field β_b for a very attractive surface, $\beta_s=8$. The lines represent results from the evaluation of the density of states for tethered chains of length $N=64$ (solid), 32 (dashed), and 16 (dash dotted).

peak at higher temperatures that indicates the transition from disordered coil conformations to disordered globule conformations, and a peak at low temperatures that indicates the transition from a liquidlike disordered globule to a solidlike ordered globule. Typically, the peak associated with the order-disorder transition, which is sometimes referred to as the "freezing" transition, sharpens with increasing chain length and is accompanied by a bimodal probability distribution as expected for a discontinuous transition. Our results for tethered and free chains show that the chain collapse in the bond fluctuation model is analogous to chain collapse in off-lattice models.

D. Chain collapse in two dimensions

If a chain is completely adsorbed to a surface, a collapse transition between two-dimensional states may be observed. To investigate this transition, we chose a strong surface field, $\beta_s=8$, and evaluated the density of states as usual, with probabilities given by Eq. (14). For comparison, we also performed calculations using only density-of-states results with the maximum number of surface contacts, $n_s=N$, and evaluated them with probabilities given by Eq. (25). For the range of β_b values relevant to the collapse transition, the results are indistinguishable. (For much higher β_b values, the transition to layered states appears in the evaluation of the full density of states but not the restricted set.) In Fig. 9 we present results for the bead-contact fluctuations χ_b of tethered chains as a function of β_b for chains of length $N=16$, 32, and 64 at $\beta_s=8$. For $N=16$, only a single maximum is discernible, while for $N=32$ the maximum is broad and accompanied by a shoulder on the high β_b side. For $N=64$, a narrower peak in χ_b is preceded by a shoulder on the low β_b side. In analogy with the two-stage collapse transition for chains tethered to a hard surface, we expect the features at low and high β_b values to indicate coil-globule and globule-globule transitions in two dimensions, respectively.

To investigate this further, we calculated the square radius of gyration R_g^2 and bond lengths B^2 of the chains. In Fig. 10 we present results for these quantities and their deriva-
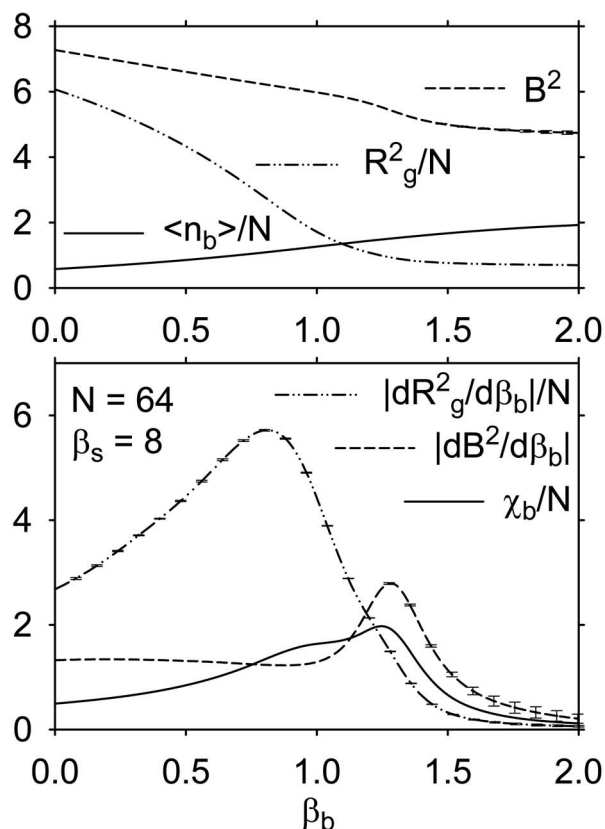

FIG. 10. Chain collapse for large surface field. The top panel shows the average square bond lengths B^2, radius of gyration R_g^2 divided by the chain length N, and the average number of monomer-monomer contacts per bead $\langle n_b\rangle/N$ as a function of the monomer-contact field β_b for a chain of length $N=64$ and a surface field $\beta_s=8.0$. The bottom panel shows how these quantities change as the chain undergoes the collapse transition. The dashed and dash-dotted lines represent absolute values of the numerical derivatives $(\partial R_g^2/\partial \beta_b)_{\beta_s}$ and $(\partial B^2/\partial \beta_b)_{\beta_s}$, respectively. The solid line represents χ_b/N as in Fig. 9.

tives with respect to β_b as a function of β_b for a chain of length $N=64$ in the surface field $\beta_s=8$. For comparison, the average number of bead contacts, $\langle n_b\rangle/N$, and their fluctuations, χ_b/N, are also shown. The graphs show that the largest changes in the radius of gyration occur near the shoulder of the χ_b graph, while the largest changes in the bond length occur near the maximum of χ_b. Since the radius of gyration measures the overall size of a chain conformation, while the bond lengths represent a small-scale property, the results suggest that a coil-globule transition is followed by a local rearrangement of segments. As in the three-dimensional case, the states beyond this latter transition are highly ordered, i.e., we interpret this "globule-globule transition" as a transition from a fluidlike to a crystal-like state. In Fig. 11(b) we show an example for such a highly ordered two-dimensional conformation of a chain of length $N=64$. As expected for an order-disorder transition, we find a bimodal probability distribution for the occupation of states at the globule-globule transition.

A two-stage transition from a disordered extended coil through a disordered globule to an ordered globule in two dimensions has also been observed in simulations with a
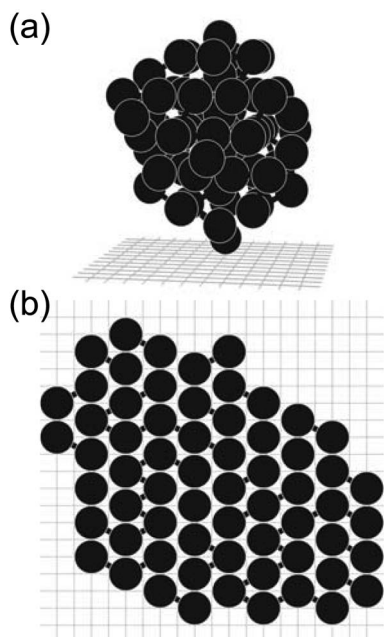
(a)

(b)

FIG. 11. Examples for compact conformations of chains of length $N=64$. (a) A highly ordered three-dimensional conformation representative of the desorbed compact (DC) region of the phase portrait in Fig. 12. (b) A highly ordered two-dimensional (single-layer) conformation representative of the adsorbed compact (AC) region of the phase portrait. In both diagrams, the size of the circles corresponds to the hard core diameter of the beads; the bonds are shown as wide lines.

FIG. 12. Phase portrait for a tethered chain of length $N=64$ in the space of the surface field (β_s) and bead-contact field (β_b). The regions are named as in Fig. 1. The solid lines represent maxima of surface (χ_s) and bead-contact (χ_b) fluctuations, as explained in the text. The dashed lines are an estimate for the location of the coil-globule transition from the "shoulder" on the susceptibility χ_b. The dotted lines represent shallow maxima in the susceptibility χ_s that depend sensitively on the details of the available compact chain conformations. In the shaded area near the center of the diagram, the susceptibility "landscapes" are too complex to identify all of the maxima clearly. This is why some of the lines end rather than merge with other lines.

parallel tempering algorithm of an off-lattice (bead-spring) model.[48] The symmetry of the two-dimensional ordered conformations is model dependent. For the BF model employed in this work, the unit cell for the ordered interior of Fig. 11(b) has basis vectors $\mathbf{a}_1=2a\hat{y}$ and $\mathbf{a}_2=a\hat{y}+2a\hat{x}$, where $\hat{x}$ and $\hat{y}$ are the unit vectors in the x and y directions, respectively, and a is the lattice constant. The number of nearest neighbors (six) is the same as for a hexagonal lattice, which is the symmetry for the two-dimensional ordered state of the off-lattice model.[48] For the ISAW model, on the other hand, compact two-dimensional chain conformations have the symmetry of the square lattice with four nearest neighbors. It is an open question to what extent these kinds of two-dimensional states carry over to chemically realistic models including rough substrates.

E. Phase portraits

In the preceding sections we have employed maxima in the susceptibilities χ_s and χ_b to identify transition fields β_s and β_b for chain adsorption in good solvent and for chain collapse near hard and very attractive surfaces. In this section, we extend this approach to a wide range of conditions and construct a phase portrait for chains of length $N=64$, shown in Fig. 12, that may be compared with the phase diagram of Fig. 1 discussed in the Introduction.

From the maxima and "shoulders" of the susceptibilities we identified transition lines in the space of field variables β_s and β_b that separate the DE, AE, DC, AC, and LS regions. The shaded area near the center of the phase portrait in Fig. 12 marks a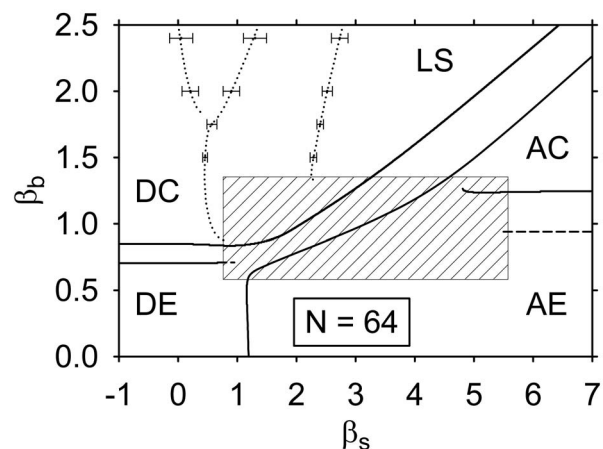 range of field values where the susceptibility "landscapes" are too complex to identify all of the maxima clearly. This is the reason why some of the lines end rather than merge with the other lines. In this discussion, we focus on field values outside the shaded area.

In the diagram of Fig. 12, the horizontal solid lines separating the DE and DC regions represent maxima of χ_b associated with the dual collapse transition in three dimensions. Similarly, the horizontal solid and dashed lines separating the AE and AC regions represent maxima and shoulders of χ_b associated with the collapse transition in two dimensions. For both collapse transitions, the fluctuations in the number of surface contacts, χ_s, are not significant. The vertical solid line separating the DE and AE regions represents maxima in χ_s associated with adsorption in good solvent. For this transition, the fluctuations in the number of bead contacts, χ_b, are small. The two solid lines that separate the regions of adsorbed states (AE and AC) from fully or partially desorbed states in poor-solvent conditions (DC and LS) represent maxima of both surface- and bead-contact fluctuations. The dotted lines in the LS region represent shallow maxima of χ_s. The error bars show the spread of the location of these maxima when different sets of density-of-states values are evaluated. The transitions associated with these maxima are structural, discontinuous transitions that depend sensitively on the details of the available compact chain conformations.

The AC states for high β_s and β_b values have strictly two-dimensional, single-layer conformations with almost hexagonal symmetry as shown in Fig. 11(b). The chain conformations for slightly lower β_s values, in the region between the two solid lines near the upper right corner of Fig. 12, have exactly two layers, each with nearly hexagonal symmetry and shifted against each other by one lattice constant a of the underlying cubic lattice. The transition from single to double layers is similar in nature to the layering

transition observed in the ISAW model. In the limit of infinite chain length, the slope of the line separating the two-layer from the one-layer conformations may be determined by equating the energy per segment of the single- and double-layer conformations.[14] For the ISAW model, the value of this slope is $1/2$. For the bond fluctuation model employed in this work, the calculated value for infinitely long chains is $1/3$ while finite size effects increase it to a value of 0.38 for the chains of length $N=64$. States in the region marked LS in Fig. 12 are very different from the single- and double-layer states discussed above. The chain conformations are three dimensional with a symmetry group corresponding to a cubic lattice with basis. The number of surface contacts decreases stepwise through the transitions marked by dotted lines until only a single surface contact is left in the region marked DC.

For the model of a tethered chain investigated in this work, all transitions from good- to poor-solvent conditions are dual in nature. The character of the transitions, continuous or discontinuous, and their dependence on the surface field β_s will be discussed in more detail in a later publication. Of course, the transitions between different states of a finite chain are no sharp phase transitions, as they occur for systems in the thermodynamic limit, but rather gradual changes in the weights of various microstates of the model system. With increasing chain length, the separation between the transition lines decreases so that a phase portrait resembles more closely the phase diagram of Fig. 1 as the chain length increases. In agreement with theoretical predictions for the ISAW,[8] we find that the transition line describing the coil-globule transition in good solvent is horizontal and perpendicular to the adsorption transition line. In contrast to the ISAW model, where the crystalline phase always has a simple cubic symmetry and the most compact conformation is cubic, the BF model supports more than one ordered phase and the most compact conformation is highly faceted. This leads to a complex sequence of transitions in the poor-solvent regime, which we will investigate in more detail in later work.

F. Relation to real polymers near surfaces

Transitions in polymers near surfaces may be induced by changing the solvent quality or, more typically, by changing the temperature. Since the BF model employed in this work orders without forming lamellae and since polymer crystallization is typically dominated by kinetic effects[22] a direct comparison with available experimental data on surface crystallization of polymers is not possible. However, we will discuss some qualitative aspects of ordered chains near surfaces. Experiments on alkanes physisorbed on graphene surfaces at low coverage show the chains to be rodlike (all trans conformations) and oriented parallel to the surface.[52,53] Experiments on thin films of a variety of crystallizable polymers show that the orientation of the chains relative to surface depends on the thickness of the layer (see, for example, Ref. 54). For very thin films, one typically finds "edge-on" lamellae corresponding to chains with their backbones oriented perpendicular to the surface. For example, for poly-(ethylene oxide) (PEO) films on bare silicon wafers, crystallites with chain backbones perpendicular to the surface grow from a layer of adsorbed, noncrystallized chains oriented parallel to the surface through a partial dewetting of the surface.[55,56]

The fields β_b and β_s employed in this work combine the inverse temperature β and the interaction parameters for net monomer-monomer interactions ϵ_b and monomer-surface interactions ϵ_b, respectively [see Eq. (12)]. In our phase portrait of Fig. 12, the origin corresponds to the limit of infinite temperature while a range of temperatures at constant interaction parameters corresponds to a segment of a straight line through the origin with the slope given by the ratio ϵ_b/ϵ_s of the interaction parameters. For example, for systems without attractive surface interactions (hard surface) a decrease in temperature moves the system up along the vertical line with $\beta_s=0$ in Fig. 12 and leads to the two-stage transition from desorbed extended to desorbed compact states. When the monomer-monomer interaction parameter ϵ_b has a much smaller magnitude than the surface interaction parameter ϵ_s, a decrease in temperature moves the system along an almost horizontal line from (0,0) to higher β_s values in Fig. 12 and leads to the adsorption transition from desorbed (DE) to adsorbed (AE) extended chain conformations. For systems where the interaction parameters ϵ_b and ϵ_s are comparable in size, our phase portrait predicts transitions from the disordered DE states to the ordered three-dimensional LS states upon lowering the temperature. While the details of the LS states clearly depend on the model, layered states are not uncommon. Off-lattice simulations of confined polymers, for example, show layered states for strong confinement[48] and the adsorption of small molecules from the vapor onto solid substrates leads to the occurrence of layered structures ("multilayer adsorption"). When the surface interactions are somewhat larger than the monomer-monomer interactions, a decrease in temperature is expected to induce chain adsorption to the disordered AE states, followed by transitions to the ordered LS states. During the ordering, the chain partially desorbs from the surface to reach the LS states. A combination of partial dewetting and ordering in a three-dimensional crystallite is also observed in experiments on PEO on silicon.[55] Finally, when the surface interactions are very strong, a transition between two-dimensional disordered (AE) and ordered (AC) states is expected from our calculations. For real polymeric systems, such strong surface attractions might be provided by specific interactions (for example, hydrogen bonding) between the surface and the polymer.

While some polymers undergo a crystallization transition as the temperature is lowered there are many polymers that remain amorphous. For example, in atactic poly(butadiene) the random distribution of monomers of different stereoregularity prevents the crystallization of the chains. In order to describe noncrystallizable polymers, one introduces an element of randomness in the composition of the model polymer. In this case, we expect the phase portrait in field space to be qualitatively the same as shown in Fig. 12 for low β_b values, but to contain single lines of continuous transitions between disordered extended and compact states. In

addition, there may be minor transitions in the compact regions corresponding to local reordering of sections of a chain.

V. SUMMARY AND CONCLUSIONS

In this work we performed Monte Carlo simulations of a bond fluctuation model for a tethered chain with two-dimensional Wang–Landau algorithms and umbrella sampling. The simulations yield density-of-states results that have been evaluated for interaction parameters spanning the range from good- to poor-solvent conditions and from repulsive to strongly attractive surfaces. For given fields β_s and β_b, we calculated expectation values for chain dimensions, contact numbers for surface- and monomer-monomer contacts, and fluctuations in the contact numbers. Three types of transitions were investigated in some detail. For adsorption in good solvent, we compared our results with Metropolis Monte Carlo data for the same model and found good agreement. For the collapse transition in three dimensions, we considered chains tethered to a hard surface and found them to behave very similar to free chains, with the differences between the two situations decreasing with increasing chain length, as expected. For the collapse transition in two dimensions, we found a dual transition with the same sequence of transitions that is observed for three-dimensional chains: a coil-globule transition that changes the overall chain size is followed by a local rearrangement of chain segments.

In order to investigate the overall phase behavior of the tethered chains considered in this work, we located maxima of the susceptibilities χ_s and χ_b in the β_s-β_b plane. We found that all transitions from good- to poor-solvent conditions are dual in nature and that the separation between the two lines belonging to the same transition decreases with increasing chain length. In agreement with theoretical predictions for the ISAW model,[8] we find that the transition line describing the coil-globule transition in good solvent is horizontal and perpendicular to the adsorption transition line. For poor-solvent conditions, early work on the ISAW model predicted the existence of a surface-attached globule (SAG) phase[11–13] which was later found to consist of a whole sequence of layered states.[14] In the corresponding parameter region we find one transition (between single- and double-layer states) that is similar to the AC to LS (SAG) transition of the ISAW. The next transition of the BF model, however, changes the symmetry of the ordered segments and has no correspondence in the ISAW model. From the maxima of the susceptibilities of finite-length chains alone it is not possible to resolve the nature of the transitions near points where transition lines meet. This is an interesting question that we will try to address in future work.

ACKNOWLEDGMENTS

TABLE II. Production parameters for chains of length $N=16$, $N=32$, and $N=64$. The table entries represent the simulation length in MC steps, where configurations are evaluated every ten MC steps. The left column indicates the type of simulation. For simulations sampling with the density of states, the number of replicas (N_r) is indicated and, in one case, the maximum number of bead contacts considered. For simulations with the Metropolis acceptance criterion, the values for the field variables β_s and β_b are shown.

N	16	32	64
$N_r=1$	1×10^8	4×10^9	3.35×10^9
$N_r=3$	1×10^9		
$N_r=4$, $n_b \leqslant 256$			2.6×10^8
$N_r=5$		1×10^9	3×10^8
$\beta_s=\beta_b=0$	1×10^9	1×10^9	1.5×10^9
$\beta_s=\beta_b=-1$			1×10^9
$\beta_s=\beta_b=-2$	2×10^9	1×10^9	4×10^8

APPENDIX: SIMULATION DETAILS

In this section, we present details of the density-of-states and production simulations for chains of length $N=16$, $N=32$, and $N=64$. For each chain length, density of states results were generated with Wang–Landau algorithms and then refined with umbrella sampling. In order to compare results from groups of simulations, the average over the $\ln(g)$ values in the interior $(N/4 < n_s < 3N/4$, $5N/16 < n_b < 25N/16)$ of the range of accessible states is calculated for each simulation and the $\ln(g)$ values are shifted by this amount. To determine uncertainties for the WL results, the average and standard deviation of the $\ln(g)$ values are calculated for each state (n_s, n_b). For umbrella sampling results, the log-density of states values are weighted by the length of the umbrella sampling simulation and the weighted average $\overline{\ln(g)}$ and standard deviation $\sigma_{\ln(g)}$ are calculated. Parameters for the umbrella sampling simulations and some numerical characteristics of the final densities of states are presented in Table I. In the following, we highlight differences in the simulations for the different chain lengths. Production was carried out either in separate simulations or concurrently with the construction of the density of states. A summary of the production simulation parameters is presented in Table II.

$N=16$. For chains of length $N=16$, four simulations with the original Wang–Landau algorithm were performed. The histogram was considered flat when the visits to each individual (n_s, n_b) state were no less than $0.8\bar{h}$, where $\bar{h}$ is the average of the visits to all states. The simulations required between 1.2×10^9 and 1.9×10^9 Monte Carlo steps to converge. The results agreed well with each other; the average, median, and maximum standard deviations of the $\ln(g)$ values are 0.017, 0.008, and 0.63, respectively. The largest deviations occur for states with the largest number of bead contacts for a given number of surface contacts, i.e., for states near the upper rim of the range of accessible states in Fig. 2. Umbrella sampling simulations with 10^9 Monte Carlo steps were performed for each of the WL density-of-states results for $N=16$ and evaluated as described in Sec. II D. The agreement between the four different results is excellent, as may be seen from the values of the standard deviations presented in Table I. As before, the largest deviations occur at the upper rim of the range of accessible states.

$N=32$. For chains of length $N=32$, simulations with the original Wang–Landau algorithm would not converge. We modified the flatness criterion and considered averages over groups of states. Each group consisted of N states and two sets of groups were created. One set was formed by going up along columns in the (n_s, n_b) plane and adding states to a group until it was filled, continuing in the next column when the top was reached before the group was complete. The other set was formed by going along rows in the same way. The histogram was considered flat when the visit to each group of states in the two sets was no less than 0.8 and no more than 1.25 of the average of the visits over all groups. We obtained results from two simulations (A and B) with a Wang–Landau algorithm where the density of states was updated only for accepted moves [see Eq. (3)] and from one simulation (C) with a five-replica Wang–Landau algorithm where the density of states was updated after accepted as well as after rejected moves, Eqs. (3) and (4). The results for the density of states from the five replicas agreed well in the regions of overlap and were combined with a simple linear switching function.

The $N=32$ simulations took between 1.3×10^{10} and 4.1×10^{10} MC steps to converge. All simulations missed or severely underestimated the density-of-states values of four states on the upper rim of accessible states in Fig. 2. Except for states on the rim, the two single-replica results A and B agree reasonably well with each other, the average, median, and maximum standard deviations of the $\ln(g)$ values are 0.029, 0.011, and 4.4, respectively. However, there are systematic deviations between the $\ln(g)$ values for high n_b-states between result C from the five-replica simulation and results A and B.

In order to prepare for umbrella sampling, the density-of-state results for $N=32$ from the Wang–Landau simulations were augmented by assigning reasonable guesses to the $\ln(g)$ values that were missed or nearly missed in the simulations. We performed umbrella sampling simulations with the parameters given in Table I and updated the density-of-states results as described in Sec. II D. The systematic deviations between results A, B, and C disappeared after umbrella sampling and the density-of-states values agree very well (see the values for the standard deviations in Table I), except for states very close to the upper rim of the range of accessible states in Fig. 2. For results A and B, umbrella sampling led to significant increases in the normalized $\ln(g)$ values for a large range of states with high numbers of bead contacts. For result C, umbrella sampling decreased the normalized $\ln(g)$ values slightly for states with very high numbers of bead contacts and changed the values significantly on the rim of accessible states. One state was not visited in the C simulation and its density-of-states value was calculated from the A and B results only. Production simulations were carried out with the parameters in Table II. For some states near the rim, production data were supplemented by evaluating stored chain conformations.

$N=64$. For chains of length $N=64$, one density-of-states result with a cutoff in the number of bead contacts at $n_b = 4N$ was obtained with the modified Wang–Landau algorithm described for chains of length $N=32$ (simulations A

and B), above. This simulation was completed in 2×10^9 MC steps; simulations without cutoff would not converge.

In order to obtain density-of-states results for a larger range of bead-contact values, we applied the global update algorithm described in Sec. II C. For the results presented here, we used the following shift parameters in Eq. (6): $\kappa = \lambda = \omega = 10^4 \ln(f_k)$, where $\ln(f_k) = 2^{-(k-1)}$ is the increment of the log-density of states at refinement level k. The first global update simulation used a value of $\rho = 10^2 \ln(f_k)$ for the uniform growth criterion. It was started at the $k=15$ level and allowed us to progress through about 8×10^8 MC steps before the refinement level was set to $k=18$. At this level, about 7.5×10^8 MC steps were carried out before our group-of-state flatness criterion was satisfied and the simulation progressed through the final two levels in a standard Wang–Landau algorithm with our flatness criterion, which took about 3.5×10^8 MC steps, for a total simulation time of about 1.9×10^9 MC steps. The density-of-states values obtained in this global update simulation agreed reasonably well in the range of common states with the results obtained in the simulation with cutoff described above. It extended the range of visited states to higher bead contacts but it missed a number of states with large surface- and bead-contact values that had been found in the simulation with cutoff. After removing states whose density-of-states values had been severely underestimated, we combined the results from the two simulations with a linear switching function; this combined density of states is referred to as result A in the following.

The second global update simulation was started at the $k=18$ level and used a value of $\rho = 10 \ln(f_k)$. With these parameters, the density of states in the interior is generated through a larger number of smaller shifts. The simulation was allowed to proceed through a total of about 3.15×10^{10} MC steps, after which time we collected the density of states, our result B. During this time, global updates and the addition of new states became increasingly rare. For example, only 31 of the more than 15 000 visited states were found in the second half of the simulation. The range of visited states from this simulation is larger than that of result A. The differences between results A and B are largest for states with very high bead-contact values; the average, median, and maximum standard deviations of the $\ln(g)$ values are 0.16, 0.1, and 18.3. In order to prepare for umbrella sampling, the density-of-state results A and B were smoothed by assigning reasonable guesses to the $\ln(g)$ values that were missed or nearly missed in the simulations.

Unfortunately, the umbrella sampling simulations for both A and B missed some states completely (20 for A and 12 for B out of a total of 15 275 input states), nearly missed a few others (8 for A and 2 for B), and found some states for the very first time (12 for A and 14 for B, with 4 in common for a total of 22 new states). All of the problematic states are very close to the upper rim of the range of accessible states shown in Fig. 2. Except for the newly found states, which were discarded, the $\ln(g)$ values were updated at the end of the umbrella sampling as described in Sec. II D. For states that were found in both umbrella sampling simulations, the log-density of states results were combined as described above. For states that had been missed or nearly missed in

one of the umbrella sampling simulations, we used the density-of-states result from the other simulation and assigned an uncertainty of $\sigma_{\ln(g)} = 1.5$. Except near the rim, the agreement between the results is very good (see Table I). Production simulations were carried out with the parameters in Table II. For some states near the rim, production data were supplemented by evaluating stored chain conformations. For 13 states on the rim, values of the quantities of interest were estimated by extrapolation from data with smaller numbers of bead contacts and generous errors were assigned. The impact of the rim states depends on the values of the field variables, in particular, on the value of β_b, as discussed in Sec. IV A. In this work, we focus on conditions where their impact is small. For future evaluation, we are currently performing simulations with a slightly modified simulation algorithm that we hope will improve the density-of-states results near the rim.

[1] D. H. Napper, *Polymeric Stabilization of Colloidal Dispersions* (Academic, London, 1983).

[2] P. Nelson, *Biological Physics: Energy, Information, Life* (W. H. Freeman, New York, 2004).

[3] A. Halperin, M. Tirrell, and T. P. Lodge, Adv. Polym. Sci. **100**, 31 (1992).

[4] M. S. Kent, Macromol. Rapid Commun. **21**, 243 (2000).

[5] C. Ray, J. R. Brown, and B. B. Akhremitchev, J. Phys. Chem. B **110**, 17578 (2006).

[6] W. Paul, T. Strauch, F. Rampf, and K. Binder, Phys. Rev. E **75**, 060801 (2007).

[7] E. Eisenriegler, *Polymers Near Surfaces: Conformation Properties and Relation to Critical Phenomena* (World Scientific, Singapore, 1993).

[8] T. Vrbová and S. G. Whittington, J. Phys. A **29**, 6253 (1996).

[9] T. Vrbová and S. G. Whittington, J. Phys. A **31**, 3989 (1998).

[10] T. Vrbová and K. Procházka, J. Phys. A **32**, 5469 (1999).

[11] Y. Singh, D. Giri, and S. Kumar, J. Phys. A **34**, L67 (2001).

[12] R. Rajesh, D. Dhar, D. Giri, S. Kumar, and Y. Singh, Phys. Rev. E **65**, 056124 (2002).

[13] P. K. Mishra, D. D. Giri, S. Kumar, and Y. Singh, Physica A **318**, 171 (2003).

[14] J. Krawczyk, A. L. Owczarek, T. Prellberg, and A. Rechnitzer, Europhys. Lett. **70**, 726 (2005).

[15] A. L. Owczarek, A. Rechnitzer, J. Krawczyk, and T. Prellberg, J. Phys. A: Math. Theor. **40**, 13257 (2007).

[16] M. Bachmann and W. Janke, Phys. Rev. Lett. **95**, 058102 (2005).

[17] M. Bachmann and W. Janke, Phys. Rev. E **73**, 041802 (2006).

[18] S. Metzger, M. Müller, K. Binder, and J. Baschnagel, J. Chem. Phys. **118**, 8489 (2003).

[19] I. Carmesin and K. Kremer, Macromolecules **21**, 2819 (1988).

[20] K. Binder, *Monte Carlo and Molecular Dynamics Simulations in Polymer Science* (Oxford University Press, Oxford, 1995).

[21] D. P. Landau and K. Binder, *A Guide to Monte Carlo Simulations in Statistical Physics* (Cambridge University, Cambridge, 2000).

[22] S. Z. D. Chen and B. Lotz, Polymer **46**, 8662 (2005).

[23] K. Binder and W. Paul, J. Polym. Sci., Part B: Polym. Phys. **35**, 1 (1997).

[24] J. Baschnagel, K. Binder, P. Doruker, A. A. Gusev, O. Hahn, K. Kremer, W. L. Mattice, F. Müller-Plathe, M. Murat, W. Paul, S. Santos, and U. W. Suter, Adv. Polym. Sci. **152**, 41 (2000).

[25] K. Binder, J. Baschnagel, M. Müller, W. Paul, and F. Rampf, Macromol. Symp. **237**, 128 (2006).

[26] E. Eisenriegler, K. Kremer, and K. Binder, J. Chem. Phys. **77**, 6296 (1982).

[27] K. De'Bell and T. Lookman, Rev. Mod. Phys. **65**, 87 (1993).

[28] S. Metzger, M. Müller, K. Binder, and J. Baschnagel, Macromol. Theory Simul. **11**, 985 (2002).

[29] R. Descas, J.-U. Sommer, and A. Blumen, J. Chem. Phys. **120**, 8831 (2004).

[30] Y. Zhou, C. K. Hall, and M. Karplus, Phys. Rev. Lett. **77**, 2822 (1996).

[31] Y. Zhou, M. Karplus, J. M. Wichert, and C. K. Hall, J. Chem. Phys. **107**, 10691 (1997).

[32] F. Rampf, W. Paul, and K. Binder, Europhys. Lett. **70**, 628 (2005).

[33] F. Wang and D. P. Landau, Phys. Rev. E **64**, 056101 (2001).

[34] D. P. Landau, S.-H. Tsai, and M. Exler, Am. J. Phys. **72**, 1294 (2004).

[35] C. Zhou, T. C. Schulthess, S. Torbrügge, and D. P. Landau, Phys. Rev. Lett. **96**, 120201 (2006).

[36] E. A. Mastny and J. J. de Pablo, J. Chem. Phys. **122**, 124109 (2005).

[37] A. Tröster and C. Dellago, Phys. Rev. E **71**, 066705 (2005).

[38] F. Rampf, K. Binder, and W. Paul, J. Polym. Sci., Part B: Polym. Phys. **44**, 2542 (2006).

[39] B. A. Berg and T. Celik, Phys. Rev. Lett. **69**, 2292 (1992).

[40] A. Mitsutake, Y. Sugita, and Y. Okamoto, Biopolymers **60**, 96 (2001).

[41] W. Janke, in *Computer Simulations of Surfaces and Interfaces*, Science Series II Vol. 114 edited by B. Dünweg, D. P. Landau, and A. I. Milchev (Kluwer, Dordrecht, The Netherlands, 2003), pp. 137–157.

[42] M. E. J. Newman and G. T. Barkema, *Monte Carlo Methods in Statistical Physics* (Clarendon, Oxford, 1999).

[43] H. B. Callen, *Thermodynamics and an Introduction to Thermostatistics*, 2nd ed. (Wiley, New York, 1985).

[44] A. Milchev, W. Paul, and K. Binder, J. Chem. Phys. **99**, 4786 (1993).

[45] H. Liang and H. Chen, J. Chem. Phys. **113**, 4469 (2000).

[46] M. P. Taylor, J. Chem. Phys. **114**, 6472 (2001).

[47] F. Calvo, J. P. K. Doye, and D. J. Wales, J. Chem. Phys. **116**, 2642 (2002).

[48] J. R. Maury-Evertsz, L. A. Estévez, and G. E. López, J. Chem. Phys. **119**, 9925 (2003).

[49] D. F. Parsons and D. R. M. Williams, J. Chem. Phys. **124**, 221103 (2006).

[50] D. F. Parsons and D. R. M. Williams, Phys. Rev. E **74**, 041804 (2006).

[51] D. T. Seaton, S. J. Mitchell, and D. P. Landau, "Developments in Wang-Landau Simulations of a Simple Continuous Homopolymer," Braz. J. Phys. (in press).

[52] R. Hentschke, L. Askadskaya, and J. P. Rabe, J. Chem. Phys. **97**, 6901 (1992).

[53] T. Arnold, R. K. Thomas, M. A. Castro, S. M. Clarke, L. Messe, and A. Inaba, Phys. Chem. Chem. Phys. **4**, 345 (2002).

[54] Y. Wang, S. Ge, M. Rafailovich, J. Sokolov, Y. Zou, H. Ade, J. Lüning, A. Lustiger, and G. Maron, Macromolecules **37**, 3319 (2004).

[55] G. Reiter and J.-U. Sommer, J. Chem. Phys. **112**, 4376 (2000).

[56] J.-U. Sommer and G. Reiter, J. Chem. Phys. **112**, 4384 (2000).